Hindawi Publishing Corporation
Advances in Materials Science and Engineering
Volume 2015, Article ID 763124, 7 pages
http://dx.doi.org/10.1155/2015/763124

Research Article

Shape-Evolution and Growth Mechanism of Fe_3O_4 Polyhedrons

Liqiao Chen,[1,2] Qiang Zhou,[2] Qingfeng Xiong,[3] Wenlin Li,[3] Jisong Liu,[3] and Xianfeng Yang[2]

[1]*Innovation & Application Institute, Zhejiang Ocean University, Zhoushan 316022, China*
[2]*State Key Laboratory of Optoelectronic Materials and Technologies, School of Chemistry and Chemical Engineering, Sun Yat-Sen University, Guangzhou 510275, China*
[3]*State Key Laboratory of Advanced Technologies for Comprehensive Utilization of Platinum Metals, Kunming Institute of Precious Metal, Kunming 650106, China*

Correspondence should be addressed to Liqiao Chen; chenlq118@126.com

Received 17 August 2015; Revised 1 November 2015; Accepted 19 November 2015

Academic Editor: Joke Hadermann

The shape evolution of spinel-structured Fe_3O_4 was systematically investigated using a one-pot solvothermal route. Using $FeCl_3 \cdot 6H_2O$ as the precursor, triangular and hexagonal plates, octahedrons, dodecahedrons, and spherical Fe_3O_4 were obtained by selecting the adequate ration of NaOH, $N_2H_4 \cdot H_2O$, Fe^{3+}, and EDTA. The slow nucleation and growth rate favor the formation of low energy plate-like products, and the spherical crystals are obtained as the result of extremely fast nucleation and growth rate. It is also suggested that the generating rate of Fe(II) reduced from Fe(III) probably affects the growth speed along different facets, further influencing the final size and shape of the produced crystals.

1. Introduction

Polyhedral micro- and nanoparticles with specific facets have attracted considerable attention because of their abundant size- and shape-dependent physical and chemical properties [1–4]. Magnetite (Fe_3O_4), a traditional material, has found many applications, such as magnetic fluids [5, 6] and microwave absorption [7, 8]. Recently, Fe_3O_4 micro- and nanoparticles with specific facets have attracted growing interest because of their unique performance in magnetic resonance imaging (MRI) [9, 10] and drug delivery [9, 11] and their catalytic and lithium storage properties [12–15]. Therefore, it remains necessary to explore more effective shape-control methods for Fe_3O_4 crystals.

From a crystallographic viewpoint, Fe_3O_4 has a cubic inverse spinel structure with oxygen anions forming a face-centered-cubic (FCC) close-packed structure. As a FCC crystal, a general sequence of surface energies may hold, $\gamma\{111\} < \gamma\{100\} < \gamma\{110\}$, which indicates that the Fe_3O_4 crystals usually exist with {111} lattice planes as the basal surfaces [16]. The difference in R, the growth rate in ⟨100⟩ to that of ⟨111⟩, results in a series of polyhedral shapes; however, the factors controlling this difference remain controversial. Zhang et al. fabricated Fe_3O_4 octahedrons and suggested that ethylenediaminetetraacetic acid (EDTA) provides the octahedral chemical environments for Fe^{3+} ions [17]. Chen et al. reported that the reaction temperature and amount of $N_2H_4 \cdot H_2O$ play important roles in determining the sizes and morphologies of the Fe_3O_4 nanocrystals [18]. Some polymers or additives were also fabricated to control the Fe_3O_4 nanocrystals [19, 20]. The results from Kumar et al. indicated that the shapes and sizes of Fe_3O_4 are controlled by adjusting the concentrations of the precursor with an invariable base medium [21]. Most of the views indicate that the pH value of the precursor solution is the key factor affecting the morphologies of the products [16]. Therefore, it remains necessary to systematically study the shape-evolution process and determine the underlying shape-evolution mechanisms for Fe_3O_4 particles.

In this study, dodecahedral, octahedral, hexagonal, and triangular plates were synthesized using a simple solution-phase route, and the shape evolution of Fe_3O_4 was systematically investigated by controlling the different conditions. Our results will enrich the controlling methods and clarify their evolution mechanism of Fe_3O_4 polyhedrons.

2. Experimental Section

Preparation. Iron trichloride ($FeCl_3{\cdot}6H_2O$, Guangdong Guanghua Chemical Co., Ltd.), EDTA [($C_{10}H_{16}O_8N_2$), Guangzhou Chemical Reagent Factory], hydrated hydrazine [$N_2H_4{\cdot}H_2O$ (85%), Sinopharm Chemical Reagent Co., Ltd.], and sodium hydroxide (NaOH, Guangzhou Chemical Reagent Factory) were of analytical grade and used as raw materials without further purification.

In a typical synthesis of Fe_3O_4 polyhedrons, 1.7 mmol EDTA was added to an 8.0 mL aqueous solution of 1.0 mmol $FeCl_3{\cdot}6H_2O$ under vigorous magnetic stirring. Then, $N_2H_4{\cdot}H_2O$ (85%) and NaOH were rapidly added to the mixture. The entire mixture was intensively stirred for another 30 min to obtain a homogeneous solution, which was sealed in a stainless-steel autoclave and maintained at 220°C for 10 h followed by natural cooling to room temperature. The resulting black solid products were rinsed with distilled water and absolute ethanol several times and finally dried in a desiccator at 60°C for 4 h for further characterization.

Characterization. The products were characterized by powder X-ray diffraction (XRD) and scanning electron microscopy (SEM). XRD patterns were recorded with a Rigaku D/MAX 2200 VPC diffractometer using Cu Kα radiation (λ = 0.15045 nm) and a graphite monochromator. SEM images were taken with a FEI Quanta 400 Thermal FE environmental scanning electron microscope. Samples were coated with gold before the SEM analysis. X-ray photoelectron spectra (XPS) were recorded on an ESCALAB 250 spectrometer to characterize the particle surfaces using an energy analyzer in the pass energy mode at 20 eV and an Al Kα line applied as the excitation source.

3. Results and Discussion

3.1. Effect of NaOH Concentration. According to many reports in the literatures [16, 17], the pH value has a great effect on the formation of Fe_3O_4 polyhedrons. To verify this claim, different conditions were implemented with NaOH additions of 2.0 mmol, 3.75 mmol, 5.0 mmol, and 12.5 mmol with a fixed dosage of hydrazine hydrate (1.5 mL). The powder X-ray diffraction (pXRD) patterns in Figure 1 match well with JCPDS Card No. 89-3854 for cubic Fe_3O_4 with $a = b = c = 8.395$ nm, confirming that all of the products are cubic-structure iron oxides. However, it is difficult to distinguish the γ-Fe_2O_3 and Fe_3O_4 phases only from the XRD patterns because of their similarity. XPS analysis (Figure 2) was performed to further ascertain the phase of the synthesized typical products (NaOH = 5.0 mmol). The binding energies relating to $Fe2p_{3/2}$ and $Fe2p_{1/2}$ are approximately 710.6 and 724.9 eV, respectively. The Fe^{2+} and Fe^{3+} signals are forming the same peak, which can be deconvoluted in the two peaks ($E \sim 708$ and 710 eV). No satellite peak between the $Fe2p_{3/2}$ and $Fe2p_{1/2}$ peaks is observed, and these are in good agreement with the results for Fe_3O_4 reported in the literature [22]. Therefore, the XPS results also confirmed the composition of Fe_3O_4.

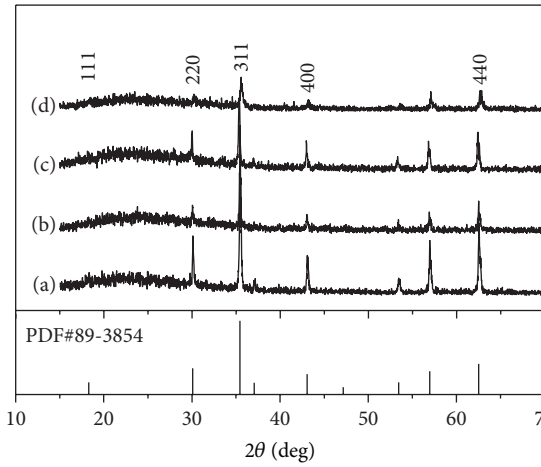

Figure 1: Powder XRD patterns of the products obtained using different amounts of NaOH: (a) 2.0 mmol (pH = 7), (b) 3.75 mmol (pH = 8), (c) 5.0 mmol (pH = 9), and (d) 12.5 mmol (pH > 14). The bars are from JCPDS Card No. 89-3854 for spinel-structured Fe_3O_4.

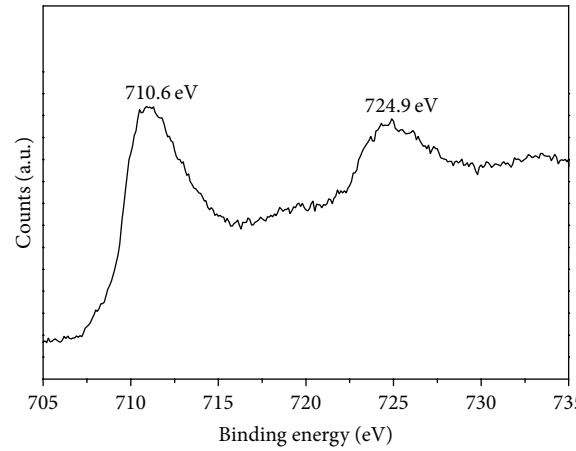

Figure 2: Fe2p XPS spectrum of as-synthesized dodecahedral Fe_3O_4 microcrystals.

The morphologies of four samples were further examined via SEM observation, and the results are presented in Figure 3. The sample synthesized with NaOH = 2.0 mmol mainly consisted of truncated octahedrons (Figure 3(a)). Octahedrons were obtained when NaOH = 3.75 mmol (Figure 3(b)). Continually increasing the amount of alkali to 5.0 mmol, the products are mainly dodecahedral structures (Figure 3(c)). Some irregular spherical-like crystals were obtained when the addition of alkali was increased to 12.5 mmol (Figure 3(d)). The sizes of the four products decreased upon increasing the alkali content, which should result from the fast nucleation and growth rate along different facets [23]. In addition, the results also reveal that, upon increasing the amount of OH^- in the solution, the Fe_3O_4 shapes transform into high-energy dodecahedrons.

3.2. Effect of $N_2H_4{\cdot}H_2O$ Dosage. Using the above-mentioned route and fixing the pH at 9, the effect of the $N_2H_4{\cdot}H_2O$ dosage was investigated in the range of 0.8–2.5 mL.

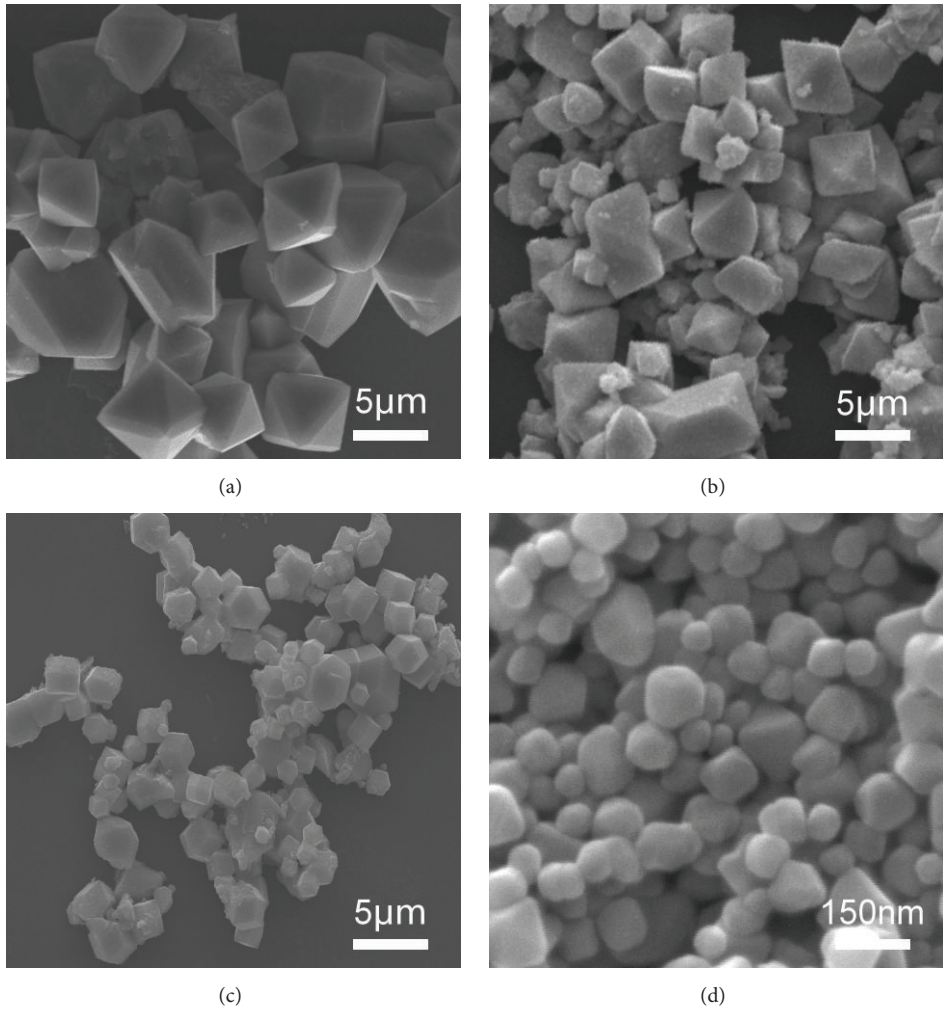

Figure 3: SEM images of samples obtained using different amounts of NaOH: (a) 2.0 mmol (pH = 7), (b) 3.75 mmol (pH = 8), (c) 5.0 mmol (pH = 9), and (d) 12.5 mmol (pH > 14).

The SEM images of the samples (Figure 4) reveal that the morphology evolution of samples was controlled from plate to octahedron to truncated dodecahedron and eventually to a complete dodecahedron upon increasing the dosage of $N_2H_4{\cdot}H_2O$ from 0.8 mL to 2.5 mL. Herein, the alkaline contents in the solution were all adjusted for pH = 9. Therefore, the experimental results indicate that the dosage of the reducing agent can also bring the shape evolution of Fe_3O_4 polyhedrons. Xuan et al. observed that the Fe^{3+} and reductant concentration of vitamin C directly affected the final morphology in the preparation of Fe_3O_4 [24]. Xu et al. also observed that an appropriate EG/H_2O ratio in the solvent is crucial for the formation of polyhedral nanocrystals [1]. Our results are consistent with these reports and indicate that a high concentration of reductant favors the formation of high-energy surface polyhedrons.

3.3. The Effect of Concentration of Fe^{3+} in the Starting Materials. Further, the effect of Fe^{3+} concentration in the starting materials was also studied for shape evolution of Fe_3O_4 through four other experiments according to the similar synthesis process; that is, the amount of $FeCl_3{\cdot}6H_2O$ is 0.05 mmol or 2.5 mmol differently. The SEM images of the as-obtained samples corresponded to Figure 5. Under the condition of the low monomer concentration ($[Fe^{3+}]$ = 0.5 mmol), the as-obtained products are dodecahedrons (Figure 5(a)). $[Fe^{3+}]$ was increased to 2.5 mmol at fixed pH = 9; some irregular polyhedrons and many small particles are found, which probably shows there are two different growth routes in the process. The irregular and big polyhedrons should be the result of Ostwald ripening, and many small particles are generated probably due to the fast nucleation rates.

Finally, we studied the effect of EDTA on the morphology at pH = 9, and the results are presented in Figure 6. In the presence of EDTA, the morphologies of the products are micrododecahedrons about 3 μm (Figure 6(a)). The morphologies changed from micrododecahedrons to nanooctahedrons in the absence of EDTA, although the nanooctahedrons are not perfect (Figure 6(b)). This result shows that EDTA not only alters the shapes of products, but also favors the formation of the bigger crystals, which is probably

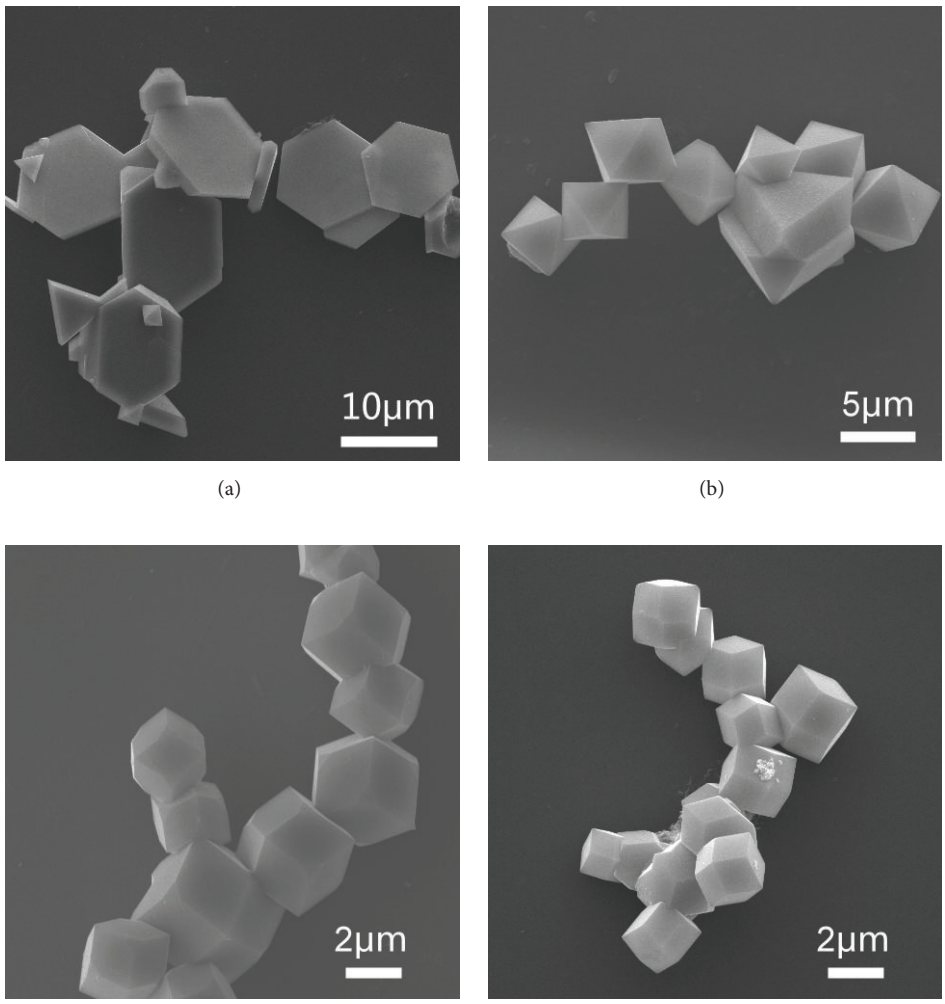

(a) (b)

(c) (d)

Figure 4: SEM images of samples obtained using different $N_2H_4 \cdot H_2O$ dosages at pH = 9 in the solution: (a) 0.8 mL, (b) 1.1 mL, (c) 1.5 mL, and (d) 2.5 mL.

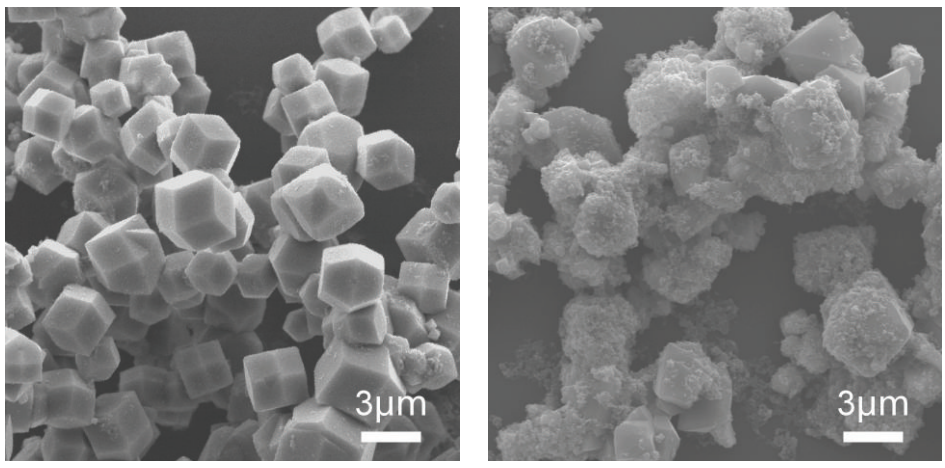

(a) (b)

Figure 5: SEM images of samples with different Fe^{3+} concentration at pH = 9, (a) $[Fe^{3+}] = 0.5$ mmol, (b) $[Fe^{3+}] = 2.5$ mmol.

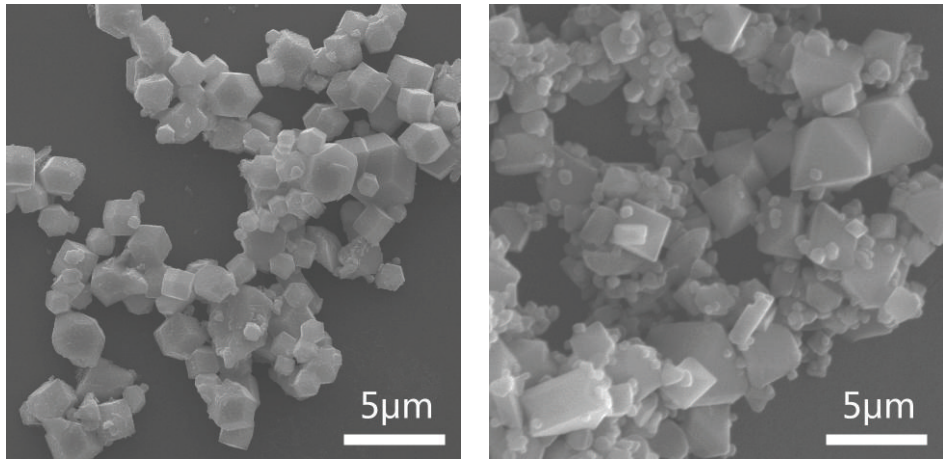

(a) (b)

Figure 6: SEM images of samples obtained in the presence of EDTA (a) and in the absence of EDTA (b) at pH = 9.

because EDTA has a strong coordinating ability with Fe^{3+} and forms a very stable complex ($K_{formation} = 10^{25}$), which reduces the nucleation and growth rate of Fe_3O_4 crystals.

3.4. Growth and Evolution Mechanism of the Different Polyhedrons. Fe_3O_4 octahedrons are surrounded by eight {111} facets, and dodecahedral crystals expose the {110} basal surfaces. The top and bottom surfaces of Fe_3O_4 triangular plates are bounded by {111} facets, and the three sides are bounded by {100} facets [25]. The exposed facets of hexagonal plates are the same as those of the triangular plates, which can be considered as the result of the alternating arrangement of six triangular plates.

Based on the experiment results, we can summarize the shape evolution mechanism of Fe_3O_4 polyhedrons as in Table 1. When the NaOH concentration was high, the growth rates on various planes are fast that the differential growth is not significant, leading to a spherical shape. Except for the spherical-like structure, the typical shapes of Fe_3O_4 in this paper also include octahedrons, dodecahedrons, and plates. The shapes and facets of the as-synthesized Fe_3O_4 crystals are sketched in Figure 7 [17, 25, 26]. In general, the facet growth rates were governed by the intrinsic surface energy. As a FCC crystal, a general sequence of surface energies may hold, $\gamma\{100\} < \gamma\{111\} < \gamma\{110\}$ in spinel oxides [23]. However, from the perspective of the growth kinetics, it is widely accepted that the growth rate of crystal facets can be controlled by experiment conditions, such as concentrations of primary materials, reaction temperature, and the surfactants. The as-grown crystal morphology is dominated by the slow-growing faces because the fast-growing faces may grow out and not be represented in the final crystal habit.

The plate-like particles expose the {100} and {111} basal surfaces, which are with lowest surface energy among all of polyhedrons in this paper, so this structure can be obtained under the lowest concentration of reducing agent. Many results have reported that a difference and change of cation site occupancy in spinel oxide result in some different structures and performances [27–30]. Fe_3O_4 has an inverse spinel structure with the formula $(Fe^{3+})A(Fe^{2+}Fe^{3+})BO_4$. Tetrahedral sites (A site, T_d) are occupied by Fe^{3+}, whereas octahedral sites (B site, O_h) are occupied by equal numbers of Fe^{2+} and Fe^{3+} in Fe_3O_4 bulk [23]. The shape-dependent occupancy of the cation sites was recently measured using X-ray magnetic circular dichroism (XMCD) spectra. Cheng observed that the different terminated planes are mainly composed of different Fe atoms and Fe(III)/Fe(II) ratios [31]. Hu et al. reported the effect of the cobalt doping concentration on the crystalline structure $Co_xFe_{3-x}O_4$ nanoparticles [32]. Therefore, in this paper, it is suggested that the generating rate of Fe(II) reduced from Fe(III) probably affects the growth speed along different facets, which further determined the shapes of the final products.

Table 1: The experiment condition and growth mechanism of typical Fe_3O_4 morphologies.

	Experiment condition	Growth mechanism
Plate	Extremely low reductant concentration	Extremely slow nucleation and growth rate
Octahedron	Low concentration of NaOH and reductant	Slow generating speed of Fe(II)
Decahedron	High concentration of NaOH and reductant	Fast generating speed of Fe(II)
Sphere	Extremely high NaOH concentration	Extremely fast nucleation and growth rate

At the same pH value, the morphological evolution of Fe_3O_4 from octahedron into high-energy dodecahedron was observed upon increasing the dosage of hydrazine because the hydrazine hydrate as a strong reducing agent increased the generating speed of Fe(II). At the same dosage of hydrazine hydrate, OH^- enhanced the hydrazine reduction ability by improving the solution chemical potential, further improving the reducing rate of Fe(III) into Fe(II) [33].

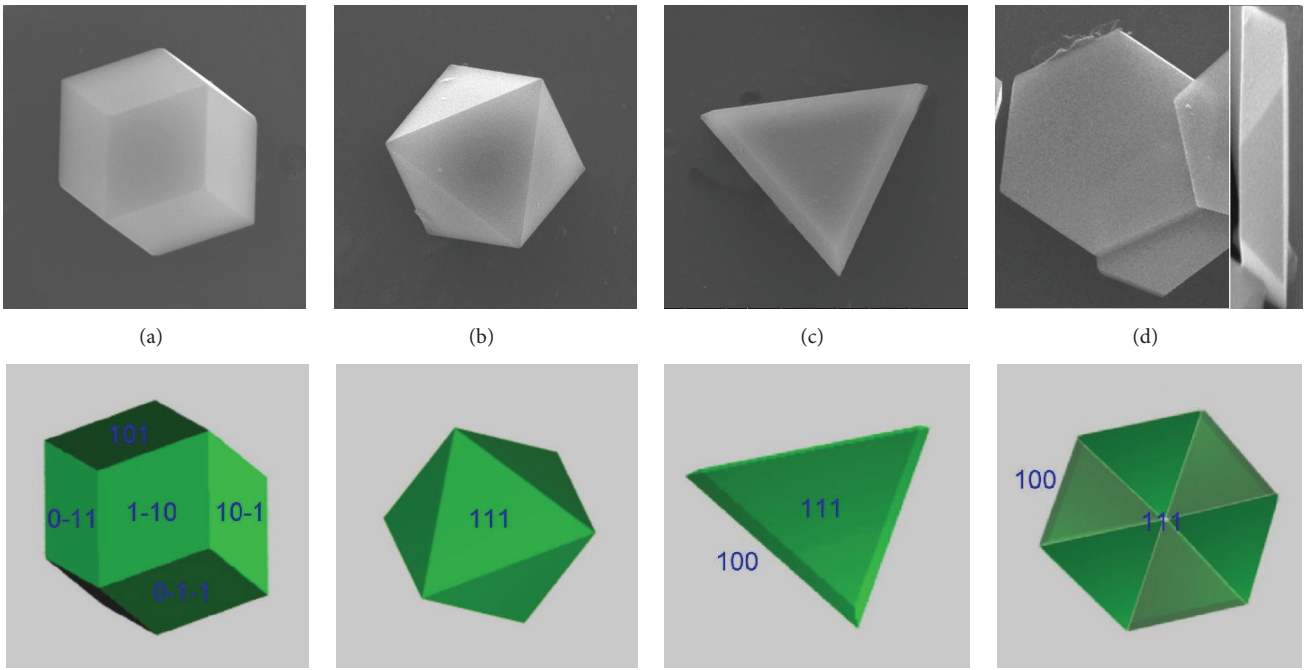

FIGURE 7: The typical morphologies in our work and sketches of the corresponding crystal structures.

Therefore, we propose that a high reducing rate of Fe(III) into Fe(II) favors the formation of the dodecahedral shape, in turn favoring the octahedron formation.

4. Conclusions

In this study, the morphological evolution of Fe_3O_4 was systematically investigated. The platy, octahedral, dodecahedral, and spherical Fe_3O_4 were synthesized through tuning the pH of the system, dosage of hydrazine hydrate, precursor concentration, and the presence/absence of EDTA. Based on the experimental results, both the nucleation and growth rate and the generating rate of Fe(II) affect the shapes and sizes of as-synthesized products. The slow nucleation and growth rate favor the formation of low energy plate-like products, and the spherical crystals were obtained as the result of extremely fast nucleation and growth rate. The fact that the different terminated planes are mainly composed of different Fe atoms and Fe(III)/Fe(II) ratios probably makes the reducing rate of Fe(III) into Fe(II) control the evolution of shape from decahedrons to octahedrons.

Conflict of Interests

The authors declare that there is no conflict of interests regarding the publication of this paper.

Acknowledgment

This work was financially supported by the National Natural Science Foundation of China (no. 51261008).

References

[1] Y. Xu, H. Hao, P. Liu, Q. Wang, Y. Sun, and G. Zhang, "Facile synthesis, shape evolution and magnetic properties of polyhedral 50-facet Fe_3O_4 nanocrystals partially enclosed by {311} high-index planes," *CrystEngComm*, vol. 16, no. 45, pp. 10451–10459, 2014.

[2] M. Song, Y. Zhang, S. Hu et al., "Influence of morphology and surface exchange reaction on magnetic properties of monodisperse magnetite nanoparticles," *Colloids and Surfaces A: Physicochemical and Engineering Aspects*, vol. 408, pp. 114–121, 2012.

[3] Z. Cheng, X. Chu, J. Yin, H. Zhong, and J. Xu, "Surfactantless synthesis of Fe_3O_4 magnetic nanobelts by a simple hydrothermal process," *Materials Letters*, vol. 75, pp. 172–174, 2012.

[4] Y. Yang, Y. Yang, W. Xiao, C. P. Neo, and J. Ding, "Shape-dependent microwave permeability of Fe_3O_4 nanoparticles: a combined experimental and theoretical study," *Nanotechnology*, vol. 26, no. 26, Article ID 265704, 2015.

[5] H. G. Cha, C. W. Kim, S. W. Kang, B. K. Kim, and Y. S. Kang, "Preparation and characterization of the magnetic fluid of trimethoxyhexadecylsilane-coated Fe_3O_4 nanoparticles," *The Journal of Physical Chemistry C*, vol. 114, no. 21, pp. 9802–9807, 2010.

[6] H. Zheng, H. P. Shao, and Z. F. Zhao, "Study on γ-Fe_2O_3 magnetic fluid by thermal oxidizing of Fe_3O_4 nanoparticles," *Applied Mechanics and Materials*, vol. 713, pp. 2916–2919, 2015.

[7] Y. Du, W. Liu, R. Qiang et al., "Shell thickness-dependent microwave absorption of core–shell Fe_3O_4@C composites," *ACS Applied Materials & Interfaces*, vol. 6, no. 15, pp. 12997–13006, 2014.

[8] G. Sun, B. Dong, M. Cao, B. Wei, and C. Hu, "Hierarchical dendrite-like magnetic materials of Fe_3O_4, γ-Fe_2O_3, and Fe

with high performance of microwave absorption," *Chemistry of Materials*, vol. 23, no. 6, pp. 1587–1593, 2011.

[9] W.-P. Li, P.-Y. Liao, C.-H. Su, and C.-S. Yeh, "Formation of oligonucleotide-gated silica shell-coated Fe_3O_4-Au core-shell nanotrisoctahedra for magnetically targeted and near-infrared light-responsive theranostic platform," *Journal of the American Chemical Society*, vol. 136, no. 28, pp. 10062–10075, 2014.

[10] Z. Zhou, Z. Zhao, H. Zhang et al., "Interplay between longitudinal and transverse contrasts in Fe_3O_4 nanoplates with (111) exposed surfaces," *ACS Nano*, vol. 8, no. 8, pp. 7976–7985, 2014.

[11] K. Cheng, S. Peng, C. Xu, and S. Sun, "Porous hollow Fe_3O_4 nanoparticles for targeted delivery and controlled release of cisplatin," *Journal of the American Chemical Society*, vol. 131, no. 30, pp. 10637–10644, 2009.

[12] X. L. Cheng, J. S. Jiang, D. M. Jiang, and Z. J. Zhao, "Synthesis of rhombic dodecahedral Fe_3O_4 nanocrystals with exposed high-energy {110} facets and their peroxidase-like activity and lithium storage properties," *The Journal of Physical Chemistry C*, vol. 118, no. 24, pp. 12588–12598, 2014.

[13] Q. An, F. Lv, Q. Liu et al., "Amorphous vanadium oxide matrixes supporting hierarchical porous Fe_3O_4/graphene nanowires as a high-rate lithium storage anode," *Nano Letters*, vol. 14, no. 11, pp. 6250–6256, 2014.

[14] D. Chen, G. Ji, Y. Ma, J. Y. Lee, and J. Lu, "Graphene-encapsulated hollow Fe_3O_4 nanoparticle aggregates as a high-performance anode material for lithium ion batteries," *ACS Applied Materials & Interfaces*, vol. 3, no. 8, pp. 3078–3083, 2011.

[15] J. Zhao, B. Yang, Z. Zheng et al., "Facile preparation of one-dimensional wrapping structure: graphene nanoscroll-wrapped of Fe_3O_4 nanoparticles and its application for lithium-ion battery," *ACS Applied Materials & Interfaces*, vol. 6, no. 12, pp. 9890–9896, 2014.

[16] L. Zhao, H. Zhang, Y. Xing et al., "Morphology-controlled synthesis of magnetites with nanoporous structures and excellent magnetic properties," *Chemistry of Materials*, vol. 20, no. 1, pp. 198–204, 2008.

[17] D. E. Zhang, X. J. Zhang, X. M. Ni, J. M. Song, and H. G. Zheng, "Fabrication and characterization of Fe_3O_4 octahedrons via an EDTA-assisted route," *Crystal Growth and Design*, vol. 7, no. 10, pp. 2117–2119, 2007.

[18] Z. Chen, Z. Geng, T. Tao, and Z. Wang, "Shape-controlled synthesis of Fe_3O_4 rhombic dodecahedrons and nanodiscs," *Materials Letters*, vol. 117, pp. 10–13, 2014.

[19] J. Sato, M. Kobayashi, H. Kato, T. Miyazaki, and M. Kakihana, "Hydrothermal synthesis of magnetite particles with uncommon crystal facets," *Journal of Asian Ceramic Societies*, vol. 2, pp. 258–262, 2014.

[20] M. H. Rashid, M. Raula, and T. K. Mandal, "Synthesis of magnetic nanostructures: shape tuning by the addition of a polymer at low temperature," *Materials Chemistry and Physics*, vol. 145, no. 3, pp. 491–498, 2014.

[21] S. R. Kumar, M. M. Raja, D. Mangalaraj, C. Viswanathan, and N. Ponpandian, "Surfactant free solvothermal synthesis of monodispersed 3D hierarchical Fe_3O_4 microspheres," *Materials Letters*, vol. 110, pp. 98–101, 2013.

[22] J. Lu, X. Jiao, D. Chen, and W. Li, "Solvothermal synthesis and characterization of Fe_3O_4 and γ-Fe_2O_3 nanoplates," *Journal of Physical Chemistry C*, vol. 113, no. 10, pp. 4012–4017, 2009.

[23] C.-H. Ho, C.-P. Tsai, C.-C. Chung et al., "Shape-controlled growth and shape-dependent cation site occupancy of monodisperse Fe_3O_4 nanoparticles," *Chemistry of Materials*, vol. 23, no. 7, pp. 1753–1760, 2011.

[24] S. H. Xuan, L. Y. Hao, W. Q. Jiang et al., "A $FeCO_3$ precursor-based route to microsized peanutlike Fe_3O_4," *Crystal Growth and Design*, vol. 7, no. 2, pp. 430–434, 2007.

[25] F.-X. Ma, X.-Y. Sun, K. He, J.-T. Jiang, L. Zhen, and C.-Y. Xu, "Hydrothermal synthesis, magnetic and electromagnetic properties of hexagonal Fe_3O_4 microplates," *Journal of Magnetism and Magnetic Materials*, vol. 361, pp. 161–165, 2014.

[26] B. Y. Geng, J. Z. Ma, and J. H. You, "Controllable synthesis of single-crystalline Fe_3O_4 polyhedra possessing the active basal facets," *Crystal Growth and Design*, vol. 8, no. 5, pp. 1443–1447, 2008.

[27] C. Wang, D. R. Baer, J. E. Amonette, M. H. Engelhard, J. Antony, and Y. Qiang, "Morphology and electronic structure of the oxide shell on the surface of iron nanoparticles," *Journal of the American Chemical Society*, vol. 131, no. 25, pp. 8824–8832, 2009.

[28] Y. Shi, P. F. Ndione, L. Y. Lim et al., "Self-doping and electrical conductivity in spinel oxides: experimental validation of doping rules," *Chemistry of Materials*, vol. 26, no. 5, pp. 1867–1873, 2014.

[29] F. Tielens, M. Calatayud, R. Franco, J. M. Recio, Pérez-Ramírez, and C. Minot, "Periodic DFT study of the structural and electronic properties of bulk $CoAl_2O_4$ spinel," *The Journal of Physical Chemistry B*, vol. 110, no. 2, pp. 988–995, 2006.

[30] H. Kim, D. H. Seo, H. Kim et al., "Multicomponent effects on the crystal structures and electrochemical properties of spinel-structured M_3O_4 (M = Fe, Mn, Co) anodes in lithium rechargeable batteries," *Chemistry of Materials*, vol. 24, pp. 720–725, 2012.

[31] C. Cheng, "Structure and magnetic properties of the Fe_3O_4 (001) surface: Ab initio studies," *Physical Review B*, vol. 71, no. 5, Article ID 052401, 2005.

[32] L. Hu, C. De Montferrand, Y. Lalatonne, L. Motte, and A. Brioude, "Effect of cobalt doping concentration on the crystalline structure and magnetic properties of monodisperse $Co_xFe_{3-x}O_4$ nanoparticles within nonpolar and aqueous solvents," *The Journal of Physical Chemistry C*, vol. 116, no. 7, pp. 4349–4355, 2012.

[33] C. Burda, X. Chen, R. Narayanan, and M. A. El-Sayed, "Chemistry and properties of nanocrystals of different shapes," *Chemical Reviews*, vol. 105, no. 4, pp. 1025–1102, 2005.